

A SILICON MODEL OF AN ADAPTING MOTONEURON

Julian A. Bragg, Edgar A. Brown, Paul Hasler, and Stephen P. DeWeerth

Georgia Institute of Technology, Atlanta, GA 30332-0363.

ABSTRACT

We have designed, fabricated, and tested an analog VLSI neuron model that exhibits many of the input-output properties characteristic of mammalian motoneurons. The circuit, which is based on an integrate-and-fire architecture, demonstrates a user-controllable recruitment threshold, a non-zero start frequency, and continuous rate adaptation across its operating range. The degree and rate of adaptation can be independently controlled. The model is suitable for use in large arrays, allowing simulation of motor pools.

The goal of this research is to create a large pool of model motoneurons in order to study biological motor control; using a phenomenological model will simplify the task of controlling the properties of the neurons in that pool. Motoneurons are the "final common pathway" of the vertebrate motor control system. They receive synaptic input from many sources (including descending fibers from the brain, pattern generators in the spinal cord, and afferent feedback from muscle sensors), and convert it into action potentials, or spikes. These spikes travel to muscle fibers and cause them to contract, generating a twitch of force. If multiple spikes occur in a short period of time, these twitches summate, yielding a sigmoidal relationship between spike frequency and muscle force.

Because motoneurons can be easily accessed in experimental preparations, they have been well studied and characterized. They have a remarkably linear steady-state current-to-frequency relationship, although they exhibit a number of nonlinear properties thought to be advantageous in motor control:

- They do not initiate firing until their synaptic input current exceeds a threshold, or *rheobase* [1]. Variation in rheobase is a critical determinant of the order in which a pool of motoneurons is activated by uniform synaptic input [2].
- Once synaptic input exceeds the firing threshold, they begin repetitive firing at a *non-zero start frequency*. Motoneurons begin firing at a rate that places them at the lower inflection point of their frequency-vs-force relationship, ensuring that subsequent increases in firing rate will cause significant increases in force output [1].
- They exhibit extremely rapid *rate adaptation*, with a step increase in current causing the neuron to fire at a high frequency for a short period of time (typically 2-3 spikes), and then reduce its firing rate to a significantly lower steady-state value [3].

Analog VLSI has been proven to be a viable medium in which to model biological neurons [4][5]. While some of these models attempt to implement mathematical models of channel populations [5][6], others use architectures that, while not mechanistically accurate, nevertheless are capable of exhibiting many characteristics of biological neurons. These *phenomenological* models are not as robust as their *mechanistic* counterparts, in that they often are valid

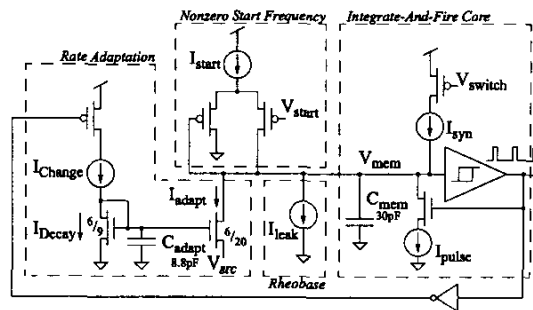


Fig. 1. A schematic of the model motoneuron. The *integrate-and-fire core* provides a basic linear current-to-frequency relationship. The *rheobase* block prevents the neuron from firing when the synaptic drive is less than a threshold current I_{leak} , while the *nonzero start frequency* block ensures firing at a nonzero frequency (set by I_{start}) once synaptic input has exceeded threshold. The *rate adaptation* block causes the neuron to be more sensitive to changes in synaptic input than to steady-state input levels. Transistor dimensions are in units of $0.3\mu m$.

only in a limited parameter space, but they have the twin advantages of being easier to understand and manipulate.

We have designed, fabricated, and tested a silicon motoneuron model that exhibits the primary input-output properties characteristic of mammalian motoneurons. This circuit, which is based on an integrate-and-fire architecture, demonstrates a user-controllable recruitment threshold, a non-zero start frequency, and continuous rate adaptation across its operating range. The degree and rate of adaptation are independently controllable. The model can be used in large arrays, facilitating the creation of motoneuron pools.

1. DESIGN OF THE MOTONEURON MODEL

Figure 1 shows the circuit schematic of the complete neuron model. The motoneuron model is based on an integrate-and-fire neuron, which linearly converts current into firing frequency [4]. By adding circuitry that alters the current flowing onto the membrane node of this basic system, we have been able to endow this relatively simple neuron with complex properties. A constant leak current provides the neuron with a *rheobase*, or threshold synaptic current; if the synaptic current onto the motoneuron is less than the rheobase, the neuron will not fire. A differential pair gives the neuron a *non-zero start frequency*, preventing it from firing at arbitrarily low rates. A diode-capacitor *adaptation circuit*, based on the work in [7], provides it with continuous rate adaptation across its entire operating range, making it more sensitive to sudden changes in synaptic current than to steady-state stimuli. By combining these circuits, we have generated a system that demonstrates the primary input-output characteristics of mammalian motoneurons, and allows direct manipulation of these characteristics.

1.1. Basic Integrate-And-Fire Dynamics

In an integrate-and-fire neuron, synaptic current (equal to the current I_{syn} , multiplied by the duty cycle of the high-frequency PWM signal V_{switch}) integrates onto a membrane capacitor C_{mem} until the capacitor voltage reaches an upper threshold voltage V_{upper} . At this point, a hysteretic element (here, a Schmitt trigger) fires, generating an output pulse that enables the reset current I_{pulse} . This reset current, which should be greater than the net current onto the membrane capacitor during integration, discharges the membrane capacitor until the capacitor reaches a lower threshold voltage V_{lower} , at which point integration resumes [4]. The total time required for the neuron to perform a complete integrate-and-fire cycle when driven by a DC current I_{syn} is given by

$$t_{total} = t_{int} + t_{fire} = \frac{Q_{mem}}{I_{syn}} + \frac{Q_{mem}}{I_{pulse} - I_{syn}} \quad (1)$$

where $Q = C_{mem}(V_{upper} - V_{lower})$, the total charge required to move the membrane capacitor from one threshold voltage to the other. Generally, I_{pulse} is large enough that the time spent in the firing state is negligible.

1.2. Addition of a Rheobase and a Non-zero Start Frequency

The rheobase circuit draws a current I_{leak} from the membrane capacitor. If the synaptic current I_{syn} is less than I_{leak} , the net current onto the membrane capacitor is negative, the membrane voltage drops below the lower Schmitt trigger threshold, and the neuron does not fire. When $I_{syn} > I_{leak}$, the net current onto the membrane capacitor is positive, and neuron fires at a rate proportional to the effective synaptic current $I_{syn} - I_{leak}$.

The non-zero start frequency circuit prevents the neuron from initiating firing at arbitrarily low rates. It consists of a differential pair that sources the current I_{start} onto the membrane capacitor when the membrane capacitor voltage exceeds the voltage V_{start} . By setting V_{start} to be slightly above the lower threshold voltage of the Schmitt trigger, we guarantee that I_{start} will be added to the effective synaptic current during repetitive firing (when the membrane voltage lies between the lower and upper thresholds), but not when the neuron is quiescent (when the membrane voltage is below the lower threshold). The magnitude of I_{start} determines the frequency at which the neuron begins firing.

1.3. Addition of Adaptation

The diode-capacitor adaptation circuit [7] transforms motoneuron firing events into an adaptation current I_{adapt} that is removed from the membrane capacitor. In this implementation, the motoneuron output is passed through an inverter, and then applied to the gate of a switching pFET. The current switched by this pFET, I_{change} , charges the capacitor C_{adapt} during firing, while the current I_{decay} discharges the capacitor during both integration and firing.

As the following analysis shows, a step increase in synaptic drive will be partially compensated for by an increase in I_{adapt} , returning the firing frequency to a somewhat lower steady-state rate. If I_{change} is sufficiently small, this compensation will take place over several spikes, resulting in gradual firing rate adaptation.

To find the dynamics of I_{adapt} , we must first find the dynamics of I_{decay} [7].

$$\frac{dI_{decay}}{dt} = BI_{decay} [I_{change} - I_{decay}] \quad (2)$$

where $B \equiv \kappa/C_c U_t$ and $U_t = kT/q$. The relationship between I_{adapt} and I_{decay} can be expressed as

$$\begin{aligned} I_{adapt} &= R_i e^{-\frac{V_{grc}}{U_t}} e^{\lambda(V_{mem} - V_{src})} I_{decay} \\ &= A e^{\lambda V_{mem}} I_{decay} \end{aligned} \quad (3)$$

where $\lambda = 1/V_A$ is the reciprocal of the Early voltage V_A of the adaptation nFET, V_{mem} is the membrane voltage, R_i is the ratio of the W/L ratios of the adaptation and decay nFETs, V_{src} is a scaling bias, and the constant A is defined as $A \equiv R_i e^{-V_{src}(\frac{1}{U_t} + \lambda)}$.

During integration, $I_{change} = 0$ and $I_{decay}(t)$ is given by

$$I_{decay}(t) = \frac{I_{decay}(0)}{1 + BI_{decay}(0)t} \quad (4)$$

where $I_{decay}(0)$ is the decay current immediately following the previous spike. By substituting this value into (3), we can find the value of I_{adapt} at t_{int} , the end of integration.

$$I_{adapt}(t_{int}) = \frac{I_{adapt}(0)}{1 + \frac{B}{A} e^{-\lambda V_{mem}(t_{int})} I_{adapt}(0)t_{int}} \quad (5)$$

Firing occurs at $t = t_{int}$ and continues until $t = t_{total} = t_{int} + t_{fire}$. During firing, $I_{change} > 0$ and $I_{decay}(t)$ is given by

$$I_{decay}(t) = \frac{I_{change} I_{decay}(t_{int}) e^{BI_{change}(t-t_{int})}}{I_{change} + I_{decay}(t_{int}) (e^{BI_{change}(t-t_{int})} - 1)} \quad (6)$$

where $I_{decay}(t_{int})$ is the decay current at the start of the action potential. If we assume that I_{pulse} is much larger than any other currents onto or off of the membrane node, the time it takes to reset the membrane capacitor following a spike can be approximated as $t_{fire} = [C_{mem}(V_{upper} - V_{lower})]/I_{pulse}$. If this firing time is short (i.e. the reset current is large, and therefore able to reset the membrane capacitor in a small period of time), (6) can be approximated to find $I_{decay}(t_{total}) = I_{decay}(t_{int} + t_{fire})$, the value of I_{decay} after an action potential has been generated.

$$I_{decay}(t_{total}) \simeq \frac{I_{decay}(t_{int})(1 + BI_{change}t_{fire})}{1 + BI_{decay}(t_{int})t_{fire}} \quad (7)$$

By substituting this value into (3), we can find the value of I_{adapt} following an action potential.

$$I_{adapt}(t_{total}) \simeq \frac{I_{adapt}(t_{int})(1 + BI_{change}t_{fire})}{1 + \frac{B}{A} e^{-\lambda V_{mem}(t_{total})} I_{adapt}(t_{int})t_{fire}} \quad (8)$$

When driven by a constant net synaptic current, the neuron eventually reaches a steady state in which the drop in I_{adapt} during integration is equal to the increase in I_{adapt} during firing. By substituting (5) into (8) and assuming steady state ($I_{adapt}(0) = I_{adapt}(t_{total})$ and $V_{mem}(0) = V_{mem}(t_{total})$), we can solve for $I_{adapt}(0)$, the value of I_{adapt} immediately following each spike. We simplify the result by noting that $BI_{change}t_{fire} \gg 1$.

$$I_{adapt}(0) \simeq \frac{AI_{change}t_{fire}}{e^{-\lambda V_{mem}(t_{int})} t_{int} + e^{-\lambda V_{mem}(0)} t_{fire}} \quad (9)$$

This result can be reduced further by noting that $V_{mem}(t_{int}) = V_{upper}$, the upper threshold voltage of the Schmitt trigger, and that $V_{mem}(0) = V_{lower}$, the lower threshold voltage of the Schmitt trigger.

$$I_{adapt}(0) \simeq \frac{AI_{change}t_{fire} e^{\lambda V_{upper}}}{t_{int} + e^{\lambda(V_{upper} - V_{lower})} t_{fire}} \quad (10)$$

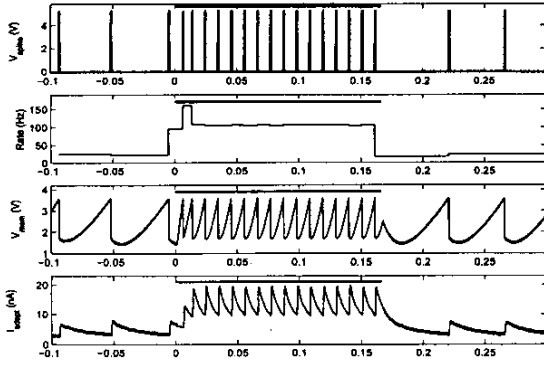


Fig. 2. Typical output from the model neuron as the synaptic drive level was stepped from 40% to 100%, and then returned to its original value. From top to bottom, the graphs present the spike output, the instantaneous firing frequency, the membrane voltage, and the adaptation current I_{adapt} . The neuron responded to the rising step by generating a short (in this case, two spikes long) high frequency burst until I_{adapt} rose to its new steady-state level. The falling step resulted in a transient drop in frequency until I_{adapt} returned to its original steady state.

2. RESULTS

The motoneuron model was fabricated through MOSIS in a $0.5\mu\text{m}$ CMOS process. During characterization, the synaptic current onto the motoneuron was controlled by gating a constant current with a high-frequency PWM signal. Because of this control scheme, which allowed the effective synaptic current to be rapidly changed in a highly repeatable manner, all drive currents are expressed as percentages of a maximum drive current.

2.1. Complete Neuron Model

Figure 2 demonstrates typical output from the neuron as its drive level was stepped from 40% to 100% of maximum drive, and then returned to its original value. For this experiment, the adaptation circuit was biased in such a way as to produce complete adaptation within two to three spikes, as is seen in biological motoneurons [3]. I_{adapt} decays as $1/t$ during the integration period, and jumps upwards during firing. Note that I_{adapt} can cause the membrane voltage to drop below the lower threshold voltage of the Schmitt trigger.

Figure 3 shows the response of the neuron as synaptic drive was stepped to different levels. The model does not fire when the synaptic input is below threshold, and when it begins to fire, it does so at a nonzero rate. The dashed lines indicate the instantaneous frequency after synaptic drive was stepped to a given drive level after being held for a prolonged period at 20%, 40%, 60%, or 80% of maximum drive, while the solid line indicates the steady-state firing frequency after the drive level has been maintained for a long period of time. The instantaneous frequency–drive relationships have a steeper slope than the steady-state frequency–drive relationship, indicating that the model is more sensitive to changes in drive level than it is to constant drive. The roll off in transient firing frequency when stepping from a high drive level to a significantly lower one is due to the lower value of I_{syn} immediately following the step; if I_{syn} is sufficiently lower than I_{adapt} , the membrane voltage will reach the lower power supply rail, moving the adaptation nFET out of saturation and attenuating the degree of adaptation.

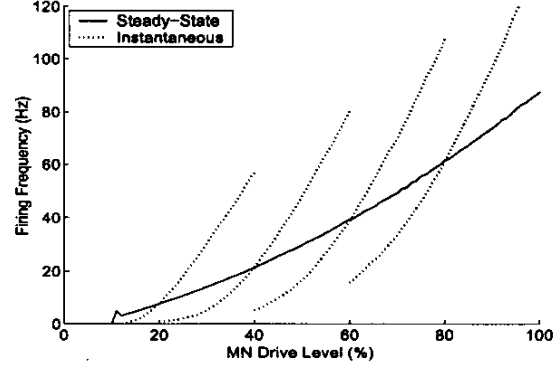


Fig. 3. Instantaneous and steady-state firing frequencies exhibited by the model in response to step changes in synaptic drive, demonstrating rheobase, nonzero start frequency, and rate adaptation. Dashed lines indicate neuron firing rate immediately after stepping from steady state (drive 20%, 40%, 60%, or 80% of maximum) to the indicated drive level.

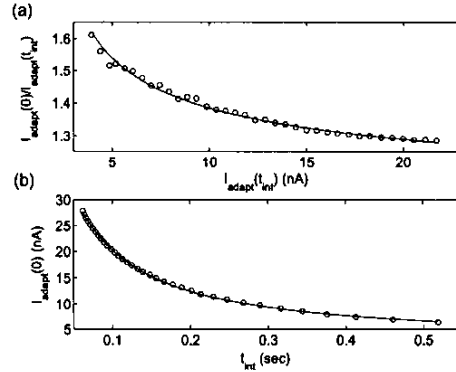


Fig. 4. (a) The proportional increase in I_{adapt} during a spike as a function of the value of I_{adapt} immediately prior to the spike while firing at steady-state. The data points are well-predicted by a curvefit to (8). (b) The peak value of I_{adapt} at steady-state as a function of the inter-spike interval. The data points are well-predicted by a curvefit to (10).

2.2. Characterization of I_{adapt}

In order to characterize the dynamics of I_{adapt} , we disabled the nonzero start frequency circuit (by setting I_{start} to zero) and drove the model neuron with varying levels of synaptic input; we then measured the timecourse of the adaptation current after the neuron had become fully adapted, and compared the value of I_{adapt} immediately prior to each spike ($I_{adapt}(t_{int})$) to the value immediately following each spike ($I_{adapt}(0)$). Figure 4(a) shows the ratio of the two currents as a function of the current prior to the spike. The curved line is a curvefit to (8).

We also compared the absolute value of $I_{adapt}(0)$, the adaptation current immediately following each spike, at steady-state over a range of synaptic inputs with the values predicted by theory. Figure 4(b) shows the value of $I_{adapt}(0)$ as a function of the inter-spike integration time (t_{int}), as well as a curvefit to (10).

2.3. Characterization of Neuronal Adaptation

To demonstrate our ability to control neuronal adaptation, we repeatedly stepped the synaptic drive from 60% to 80% of max-

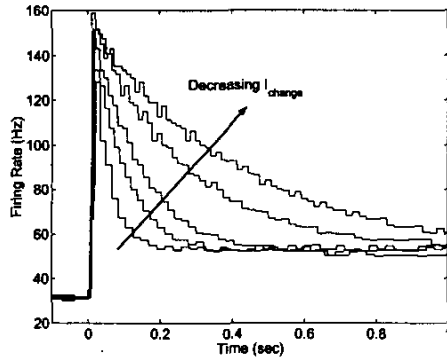


Fig. 5. Firing rate vs. time after a step in synaptic drive for trials with steady-state firing rates near 50Hz. As I_{change} decreases, the rate of adaptation decreases.

imum, while varying V_{src} and V_{change} (the voltage on the gate of the pFET producing I_{change}), and observed a range of steady-state firing rates. Figure 5, which shows firing rate vs. time for a number of trials with steady-state rates near 50Hz, demonstrates a wide range of adaptation time constants. We noted that increasing V_{change} (which reduces I_{change}) caused the speed of adaptation to decrease.

To characterize the effects of V_{src} and V_{change} on the depth and rate of adaptation, we extracted these characteristics from each trial in the dataset. Depth of adaptation was defined as the peak firing rate after the step in drive level divided by the steady-state firing rate, while rate of adaptation was defined as the time constant of an exponential decay fitted to the rate vs. time relationship of each trial. Figure 6 demonstrates that the depth of adaptation is a function of both V_{src} and V_{change} , while the adaptation rate is dependent only upon V_{change} . This independence allows the parameters of adaptation to be easily tuned by first adjusting V_{change} until the time constant is as desired, and then adjusting V_{src} to tune the depth of adaptation.

2.4. Interaction of Nonzero Start Frequency and Adaptation Elements

The current implementation of the nonzero start frequency circuit interacts with the adaptation circuit in ways which cause the model to deviate from desired behavior in certain regions of operation. If the threshold voltage for the nonzero start frequency circuit (V_{start}) is placed slightly above the lower threshold of the Schmitt trigger, then high levels of I_{adapt} can cause I_{start} to be shut off immediately following a spike. This leads to unpredictable behavior in the neuron, including the development of a doublet firing pattern (groups of two spikes close together, with long pauses between them) at low synaptic drive levels. Placing the threshold voltage well below the Schmitt trigger threshold leads to a case where the neuron does not stop firing at subthreshold drive levels, since I_{start} is always being sourced onto the membrane. In the extreme case, where $I_{start} > I_{leak}$, the only way to stop the motoneuron from firing once it has begun generating spikes is to allow it to reach steady state at a high level of synaptic drive, and then rapidly reduce the drive level below the firing threshold; the high value of I_{adapt} immediately after the downgoing step can be sufficient to drop the membrane voltage below V_{start} and stop the neuron from firing.

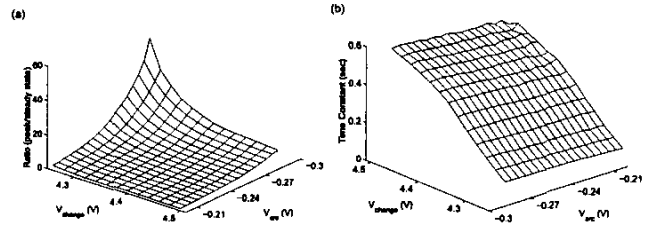


Fig. 6. (a)Depth of adaptation as a function of V_{src} and V_{change} . The depth of adaptation is increased by decreases in either V_{src} or V_{change} . (b)Adaptation rate (time constant of an exponential fit to the rate-time relationship) as a function of V_{src} and V_{change} . The rate of adaptation is increased by decreasing V_{change} , and is effectively independent of V_{src} over the tested range.

3. CONCLUSIONS

We have implemented an analog VLSI neuron model that exhibits the primary characteristic properties of a mammalian motoneuron. Rather than attempting to represent the mechanics underlying these properties, this model implements them directly by adapting a core integrate-and-fire architecture. While the resultant system does not offer any true insight into the physiology of the motoneuron itself, it is easy to understand and control. This makes the model suitable for use as a building block in the construction of more complex sensorimotor systems, especially those requiring large arrays of motoneurons.

4. REFERENCES

- [1] D.Kernell, "Spinal motoneurons and their muscle fibers: Mechanisms and long-term consequences of common activation patterns," in *The Segmental Motor System*, M.D.Binder and L.M.Mendell, Eds., pp. pp. 36-57. New York, NY: Oxford University Press, 1990.
- [2] M.J.Pinter, "The role of motoneuron membrane properties in the determination of recruitment order," in *The Segmental Motor System*, M.D.Binder and L.M.Mendell, Eds., pp. 165-181. New York, NY: Oxford University Press, 1990.
- [3] R.Granit, D.Kernell, and Y.Lamarre, "Algebraical summation in synaptic activation of motoneurons firing in the 'primary range' to synaptic currents," *J. Physiol. (Lond.)*, vol. 187, pp. 379-399, 1966.
- [4] Carver Mead, *Analog VLSI and Neural Systems*, New York, NY: Addison-Wesley, 1989.
- [5] M.Mahowald and R.Douglas, "A silicon neuron," *Nature*, vol. 354, pp. 515-518, 1991.
- [6] M.Simoni and S.DeWeerth, "Adaptation in a vlsi model of a neuron," *IEEE Transactions on Circuits and Systems II*, vol. 46, no. 7, pp. 967-970, 1999.
- [7] K.A.Boahen, "The retinomorph approach: Pixel-parallel adaptive amplification, filtering, and quantization," *Analog Integrated Circuits and Signal Processing*, vol. 13, no. 2, pp. 53-68, 1997.